Discovery of New AKT1 Inhibitors by Combination of In silico Structure Based Virtual Screening Approaches and Biological Evaluations

Filip Fratev,[†,‡] Denisse A. Gutierrez,[¶] Renato J. Aguilera,[¶] and Suman Sirimulla[*,†]

†*Department of Pharmaceutical Sciences, School of Pharmacy, The University of Texas at El Paso*

‡*Micar 21 Ltd., 34B Persenk Str., 1407, Sofia, Bulgaria*

¶*Department of Biological Sciences, The University of Texas at El Paso*

E-mail: ssirimulla@utep.edu

Abstract

AKT1 is emerging as a useful target for treating cancer. Herein, we discovered a new set of ligands that inhibit the AKT1, as shown by *in vitro* binding and cell line studies, using a newly designed virtual screening protocol that combines structure-based pharmacophore and docking screens. Taking together with the biological data, the combination of structure based pharamcophore and docking methods demonstrated reasonable success rate in identifying new inhibitors (60-70%) proving the success of aforementioned approach. A detail analysis of the ligand-protein interactions was performed explaining observed activities.

Keywords: AKT1, Virtual screen, Pharmacophore, Docking, structure-based drug discovery

Introduction

AKT, also known as protein kinase B (PKB), is a serine/threonine kinase that exists in three homologous human isoforms (AKT1, AKT2 and AKT3). AKT isozymes play significant roles in apoptotic pathways and signal transduction, and therefore, influence cellular survival and proliferation.[1–3] AKT over-expression exerts considerable anti-apoptotic effects in many cell types.[1–3] Many cancers (e.g., breast, ovarian, prostate carcinomas and glioblastomas) were found to involve mutation or loss of the AKT negative regulator PTEN.[1,2] Accordingly, inhibiting AKT signaling is a promising approach toward managing many cancers.[4–7] Several *in silico* virtual screenings (VS) have been already used, followed by *in vitro* experiments, to discover new classes of AKT1 inhibitors. For instance, Dong et al.[8] combined ligand-based pharmacophore and docking studies to identify nine promising hits. Biological testing of six of these leads indicated inhibition, and IC_{50} values between 3.9 and 143.9 μM. Cell line tests on two of these ligands indicated apoptosis. Alternatively, Chuang et al.[9] employed solely structure-based docking. From 48 promising candidates, 12 compounds displayed comparable or more potent cytotoxic activity compared to the reference compound, H-89, against HCT-116 colon cancer cells. The best results came from compounds a46 and a48: IC_{50} values of 201 and 158 μM, respectively. Compound a48 showed 75% inhibition at 100 μM concentration. Al-Sha're et al.[10] used pharmacophore/quantitative structure–activity relationship (QSAR) modeling to identify optimal binding models and found new dual AKT3/AKT1 inhibitors. All 40 tested hits fit a pharmacophore model. Unfortunately, only six of them exhibited anti-AKT3 and/or AKT1 bioactivities.

Thus, as previously suggested,[11] combining ligand-based pharamcophore and docking studies results in more success than either approach alone. Researchers have applied similar methods to search for new AKT2 and AKT3 inhibitors.[10,12] Herein, we have identified and characterized new AKT1 inhibitors. We used a VS protocol that combines structure-based pharmacophore and docking screens, and we tested our results against biochemical assays.

Methods

Virtual Screening

A combination of structure- and ligand-based approaches provides superior results for drug discovery *in silico*, relative to using either approach alone.[11] However, for many targets there are no (or limited) ligands available, thus rendering this combination impossible. In these cases, structure-based pharmacophore models could be of great help and should be intensively tested.

Herein, we tested whether a recently introduced structure-based pharmacophore approach in Phase software (Schrödinger package), in combination with docking followed by rescoring with the new Glide-SP scoring function, can achieve reasonable virtual screening (VS) results. We tested this approach on the full (102 targets) DUD-E benchmark. Surprisingly, we found that the structure-based pharmacophore hypothesis (an evaluation of the docking of more than 600 small fragments; the default number in Phase) performs well for most of the targets, with an average active ligand recovery rate of 10%–15% during the first 1% database screen.[13] The MD-prepared structures further increased these values. These results are equivalent to the ligand-based pharmacophore VS. The docking technique performed much better on the DUD-E set. Early enrichment performance shows on average of approximately 30% of known activities are recovered in screening the top-ranked 1% of recovered decoys, similarly to the previous DUD test results. Furthermore, we confirmed an improvement of the Glide-SP scoring function, as claimed on Schrödinger website, as it is shown on the ACE test target, which usually produced unsatisfied results in previous reports (Figure S14 in Fratev et. al.[14]).

However, the primary aim of a real drug discovery project is very early enrichment performance; i.e., how many active compounds will be discovered in the top 10 to 50 ligands, which we term the success rate (SR) or efficiency (EF). According to our data, combining these methods achieves an impressive result: a nearly 75% success rate for all 102 targets,

often reaching 100%, for the top 10 ligands.[13] Based on our data, we developed a new VS protocol using the top 10% of the pharmacophore search (3.5 million ZINC compounds in our case) as an input to the docking and scoring by Glide-SP (35,000 ligands). We performed all calculations using Schrödinger's Phase and Glide software packages, as implemented in Schrödinger 2017-4 suite.[15] Our approach may advance drug discovery, and we have already applied it toward the discovery of GlyT2 transporter inhibitors.[14]

Structure and ligand preparation

We used the structure of AKT1 in complex with an inhibitor (PDB ID: 3QKK) as the basis for our *in silico* studies. We undertook X-ray structure preparation for subsequent modeling with Protein Preparation Wizard. We added missing atoms and the hydrogen bonding network by assigning tautomer/ionization states, sampling water orientations, and flipping Asn, Gln, and His residues in the plane of their π-systems. All resolved crystal water molecules were deleted. Ligand 3D structures were loaded as SDF files from the ZINC library.

Pharmacophore and docking

As aforementioned, we used a combination of structure-based pharmacophore and docking approaches as implemented in Schrödinger Suite 2017-4. We employed the default setting for both of these methods. An exception was that during the docking we kept 10,000 (instead of 5,000) initial docking poses, and we employed the rewards of hydrogen bonds as an option.

***In vitro* binding assays**

All compounds are commercially available and were purchased from Sigma-Aldrich. A FRET-based Z'-LYTE kinase assay was performed by Thermofisher Inc. Briefly, all Peptide/Kinase Mixtures are diluted to a 2X working concentration. The 2X AKT1 (PKB alpha) / Ser/Thr 06 mixture is prepared in 50 mM HEPES pH 7.5, 0.01% BRIJ-35, 10

mM MgCl2, 1 mM EGTA. The final 10 μL Kinase Reaction consists of 0.82 - 12 ng AKT1 (PKB alpha) and 2 μM Ser/Thr 06 in 50 mM HEPES pH 7.5, 0.01% BRIJ-35, 10 mM MgCl2, 1 mM EGTA. After the 1 hour Kinase Reaction incubation, 5 μL of a 1:4096 dilution of development reagent is added. The tested compounds were screened in 1% DMSO (final) in the well. The IC_{50} of Compound 1 was obtained after activity measurements in ten different concentrations. For 10 point titrations, 3-fold serial dilutions were conducted from the starting concentration of 2 nM. The activity of all other ligands was obtained only for 10 and 100 μM concentrations. More details about the protocol and assay conditions can be found here: http://assets.thermofisher.com/TFS-Assets/BID/Methods-&-Protocols/20180123_SSBK_Customer_Protocol_and_Assay_Conditions.pdf

Cytotoxicity assay

To evaluate the cytotoxic activity of the compounds presented in this study, the previously validated Differential Nuclear Staining (DNS) assay was used.[16,17] The acute lymphoblastic leukemia CEM (ATCC, Manassas, VA) cells were plated at a density of 10,000 cells per well in 100 L of culture media (RPMI-1640 supplemented with 10% FBS and 1% penicillin-streptomycin) in black flat-bottomed plastic 96-well plates (BD Biosciences, Rockville, MD). 24 h later cells were treated with increasing concentrations of each compound; from 0.1 to 7.5 M final concentrations (diluted in 1% DMSO). As a vehicle and positive control for death, cells were treated with 1% DMSO and 1 mM of H2O2 respectively. Untreated cells were also included as viable cell controls. Each experimental point was included in triplicate. Treated cells were incubated for 48 h, at 37 C in humidified 5% carbon dioxide (CO2) atmosphere. Two hours prior the end of the incubation period, cells were stained with a mixture of Hoechst 33342 (Invitrogen, Eugene, OR, USA) and Propidium iodide (PI; MP Biomedicals, Solon, OH, USA) at a final concentration of 1 g/ml for each dye and incubated for 2 h. Hoechst permeates and stains the nuclei of healthy and dead cells, whereas PI permeates only the cells with compromised membranes, defined as dead cells, to subsequently stain their nuclei.

Image acquisition was performed using the IN Cell Analyzer 2000 bioimager system (GE Healthcare, Pittsburg PA, USA) acquiring four contiguous images per well, generating 2X2 montages, using a 10x objective, from two fluorescent channels (Hoechst; 453 nm and PI; 617 nm emission signals). To obtain percentages of live and dead cells, image analysis was accomplished by using the IN cell Investigator workstation 3.2. In this assay, cells positive for Hoechst (blue) are counted as the total number of cells in the captured images, whereas cells positive for both dyes, Hoechst and PI (red), are recognized as the dead cell population.

Results and discussion

In silico Virtual screening

Toward discovering new AKT1 inhibitors, we developed a special protocol for our high-throughput virtual screening (HTVS). We combined a recently introduced structure-based pharmacophore approach with the docking method in the framework of the Schrödinger 2017-4 package.[13–15] This type of pharmacophore model is based on the docking of several hundred fragments into the binding site (specifically, the AKT1 ATP binding pocket). The pharmacophore points are defined in accordance with their best position . These are the places within the binding site that were predicted to be essential for ligand binding (Figure 1 A). Eight point pharmacophore model was created for our VS study (Figure 1 B). This model requested a presence of an aromatic ring with both acceptor and donor capable substituents at the upper part of the ATP binding site, aromatic and/or hydrophobic core, along with a donor, at the center and also an aromatic rings that would be able to interact with the loop residues at the lower end of the binding pocket. We used the default settings (albeit four matched pharmacophore points, not all eight), to test the success of the structure-based pharmacophore approach when information on ligand–protein interactions is limited. However, this could be further refined based on more AKT1's specific key structural features.

Initital screening was done on 3.5 million compounds from the ZINC15[18] library via the

developed pharmacophore model. Further, the top 35,000 best candidates were subjected to docking, using the Gide SP scoring function, and finally top-scoring 100 ligands were visually inspected and nine promising candidates with scores of at least approximately $-9kcal/mol$ were chosen for biological evaluation.

We initially developed and tested our approach on the DUD-E dataset.[13] The DUD-E results for AKT1 (Figure 2) gave a recovery (success) rate of the active ligands, versus decoys, of 100%, 90%, and 76% for the top 10, 20, and 50 ligands, respectively. Furter, We successfully applied our protocol during HTVS for identifying new glycine 2 transporter inhibitors(GlyT2), and discovered several hits with submicromolar activity. The best hit had an IC_{50} value of 0.48 μM against human GlyT2 protein.[14]

In vitro binding assay and Cytotoxicity in human cancer cell lines

The potential anticancer activity of the proposed molecules were evaluated for 1)their AKT1 binding affinity using *in vitro* binding assays and 2)cytotoxicity using human cell line experiments. Initially, the selected nine compounds (Figure 3 shows the structures, ZINC number, and docking score of the slected compounds)were tested with *in vitro* single-point AKT1 binding assay at 10 μM concentration and also cell line experiments were performed for them in the acute lymphoblastic leukemia cell line; CEM by a differential nuclear staining assay. The cell line assay consists on performing live cell imaging of a treated population to determine cell viability. Cells were exposed for 48 h to a gradient of concentrations of the compounds ranging from 0.1 to 7.5 M. Thereafter, images were acquired and analyzed to obtain percentages of live and dead cells(See Methods section).

Five of these ligands(compounds 1, 2, 5, 6, and 13) showed an AKT1 inhibition of more than 10% at 10μM; further testing was done at 100 μM concentration (Table 1). As shown in figure 4A, the CEM cells exhibited differential amounts of cytotoxicity against the different compounds tested. Compounds 1, 2, 3, 7, and Z22 displayed a slight cytotoxic activity at 5 μM, with values below 15 % of cell death. Moreover, compounds 4, 5, 6 and Z18

demonstrated the highest cytotoxic values at the aforementioned concentration on CEM cells; 19.69%, 29.74%, 22.83% and 19.14%, respectively (Figure 4A). Those four compounds were selected to construct the dose-response curves (Figure 4B). Also, compound 5 and 6 maintained the uppermost values throughout the range of experimental concentrations (Figure 4B). Interestingly, compound 6 was found to be one of the strongest AKT inhibitors tested in this study (Table 1), presenting 45% of inhibition at a 100 μM.

Table 1: Observed biological activity of tested compounds. Each experimental value is a mean of two independently performed tests.

Compound Name	%Inhibition at 10 μM mean	%Inhibition at 100 μM mean	Cell inactivity at 7.5 μM
1	22	76	No
2	11	47	No
3	4	n/a	Yes
4	6	n/a	Yes
5	12	26	Yes
6	29	45	Yes
7	7	n/a	No
z18	13	27	Yes
z22	8	n/a	No

Compounds 3 and 4 were active in the cell line measurements, but were not even modest AKT1 inhibitors. Compound 1 showed the highest AKT1 activity (76% inhibition at 100 μM), and our 10 points measurements indicated an IC_{50} value of 46.4 μM (Figure 5). Compound 2 showed also modest yet considerable inhibition: approximately 50% at 100 μM. However, compounds 1 and 2 did not exhibit any considerable activity in our cell line experiments, at concentrations of 7.5 or 50 μM. This may be attributable to the low ligand concentration (no apoptosis). Compounds 1 and 2 may be more selective to AKT1, whereas compounds 3 and 4 may be much more active to other kinases from this class (AKT2/3, PKA, PKC, and so on). This may explain the considerable cellular lethality, typical to some much stronger inhibitors. For instance, research suggests that compound 3 may also be an EPHB4 inhibitor. Knockdown of EPHB4 inhibits phosphatidylinositol 3-kinase/AKT

signaling, accompanied by a reduction in cell viability.[19] Cell viability can be rescued by a constitutively active form of AKT, thus explaining the activity in our cell line experiments. Another example is compound z18, which showed weak AKT1 activity yet produced significant tumor cell apoptosis (nearly 40% at 50 μM concentration). The literature predicts this compound to also be a GPR91 (succinate receptor 1) inhibitor, which is pertinent to the PI3K/Akt/mTOR pathway via upregulation of VEGF[20].[21] Thus, one can expect this compound to exhibit a synergetic effect, in that it can bind to other proteins in the AKT signaling cascade. We are currently testing this hypothesis in our laboratory.

Thus, finding selective ligands via VS is challenging, necessitating a combination of cell line and binding experiments. Binding tests of a panel with many more kinases will also be helpful. Additional selectivity and activity improvements can be achieved relatively easily by more advanced *in silico* methods, such as free energy perturbation (FEP) and especially FEP+[22].[23]

Our compounds exhibited a plateau curve; i.e., similar cell death above a given ligand concentration (Figure 4 B). This is typical of ATP-competitive inhibitors and differs from our reference ligand, API-1, which features allosteric AKT1 binding (Figures 1B and 1C in Severson and Meyer paper[24]). For instance, the highly potent GSK690693 agent (IC_{50} of 2 nM) resulted in approximately 20% cell mortality at $\geq$0.5 μM. Thus, our cell line experiments provided an additional experimental validation that our new hits bind to the ATP pocket.

Interestingly, the IC_{50} values of new hits in most of VS studies were at greater than 50–100 μM. One of the reasons is that we omitted the presence of natural peptide. Furthermore, our pharmacophore model was the default model; i.e., we did not improve it based on specific AKT1 structural features or expert opinion. For instance, the aromatic points R42 and R43 (Figure 1 B) could be deleted, the number of pharmacophores could be reduced only to the most significant, and most importantly the requested number of matches could be set more strictly and increased. However, one of our aims in this study was to evaluate also the default performance of the method as it is implemented in Schrödinder package and requested 4 of

8 pharmacophore point's match. Our experience demonstrated that matching all points is the best approach and we highly recommend it.[14]

Structural basis of the observed activity

The compound 6 structure is typical for an AKT inhibitor. It has a purine core attached to piperazine. However, the indazole ring may be too big to fit well and interact with the P-loop, in particular Phe161 (Figure 6). Compound 2 has similar structural features and almost identical interactions at the upper part of the ATP binding pocket (Glu228 and Ala230). It also forms hydrogen bonds with Glu234 and Glu278, but does not contact the loop and exhibits only moderate activity, proving that interactions with the loop residues are an important factor for binding (Figure 7). This has been demonstrated in structure activity optimization studies,[25] and is also evident from data of compound 4. The last ligand provides neither stable contact with the loop residues nor with those from the other side of the binding grove, and the activity was completely lost. This also provides additional information for further SAR studies. Thus, appropriate optimization, guided by approaches such as FEP+, may greatly enhance the activity. On the other hand, the ring of the most active ligand, compound 1, exhibits interactions along the ATP binding pocket and forms several hydrogen bonds within the loop (residues Phe161 and Gly162), which contributes to its activity (Figure 8).

Conclusions

Our data demonstrates that a combination of structure-based pharmacophore and docking approaches was successful in discovering new potential AKT1 inhibitors. When we combined the binding and cell line data, we obtained a reasonable success rate of identifying new hits (60%–70%). However, during the pharmacophore search the choice of a model matching more features, e.g. more specific and significant potential ligand-protein interactions, seems to be critical for both activity and selectivity in identifying new hits. Recently, we identified also

highly potent ($\leq$0.5 μM) glycine transporter 2 leads in this manner.[14] Thus, our approach is useful for VS when (1) no ligands are known for a target, (2) the number of ligands is limited, or (3) a conventional ligand-based pharmacophore search is infeasible.

Acknowledgement

The authors thank the High- Performance Computing support staff (Marc T. Hertlein and Leopoldo A. Hernandez) at The University of Texas at El Paso for assistance in using the Chanti cluster. The authors thank the Cytometry, Screening and Imaging Core Facilities at the University of Texas at El Paso (UTEP), which are supported by a Research Centers in Minority Institutions (RCMI) program grant 5G12MD007592 to the Border Biomedical Research Center (BBRC) in UTEP from the National Institute on Minority Health and Health Disparities. The authors also thank Ricardo Avila and Michael Scott Long for reading and editing the paper.

Funding

This work is supported by Dr. Suman Sirimulla's startup fund from UTEP School of Pharmacy.

Author Contributions

SS conceived and supervised the project. FF performed all the Computational Work. DG performed the human cell line cytotoxicity assays and RA supervised it. FF and SS wrote the manuscript. All others contributed to the analysis of results, reviewed, and edited the manuscript.

References

(1) Siegel, R.; Ma, J.; Zou, Z.; Jemal, A. *CA: a cancer journal for clinicians* **2014**, *64*, 9–29.

(2) Nitulescu, G. M.; Margina, D.; Juzenas, P.; Peng, Q.; Olaru, O. T.; Saloustros, E.; Fenga, C.; Spandidos, D. A.; Libra, M.; Tsatsakis, A. M. *Int J Oncol* **2015**, *48*, 869–885, 26698230[pmid].

(3) Bhutani, J.; Sheikh, A.; Niazi, A. K. *Infectious Agents and Cancer* **2013**, *8*, 49.

(4) Carnero, A. *Current pharmaceutical design* **2010**, *16*, 34–44.

(5) Blake, J. F. et al. *Journal of Medicinal Chemistry* **2012**, *55*, 8110–8127, PMID: 22934575.

(6) Pal, S. K.; Reckamp, K.; Yu, H.; Figlin, R. A. *Expert Opin Investig Drugs* **2010**, *19*, 1355–1366, 20846000[pmid].

(7) Freeman-Cook, K. D. et al. *Journal of Medicinal Chemistry* **2010**, *53*, 4615–4622, PMID: 20481595.

(8) Dong, X.; Zhou, X.; Jing, H.; Chen, J.; Liu, T.; Yang, B.; He, Q.; Hu, Y. *European Journal of Medicinal Chemistry* **2011**, *46*, 5949–5958.

(9) Chuang, C.-H.; Cheng, T.-C.; Leu, Y.-L.; Chuang, K.-H.; Tzou, S.-C.; Chen, C.-S. *International Journal of Molecular Sciences* **2015**, *16*, 3202–3212.

(10) Al-Sha'er, M. A.; Taha, M. O. *Journal of Molecular Graphics and Modelling* **2018**, *83*, 153–166.

(11) Peach, M. L.; Nicklaus, M. C. *J Cheminform* **2009**, *1*, 6–6, 20298524[pmid].

(12) Medina-Franco, J. L.; Giulianotti, M. A.; Yu, Y.; Shen, L.; Yao, L.; Singh, N. *Bioorganic & Medicinal Chemistry Letters* **2009**, *19*, 4634–4638.

(13) Fratev, F.; Rivera, M.; Sirimulla, S. Efficient structure-based protocol for lead identification. Techincal abstracts of the South West Regional Meeting American Chemical Society. 2017.

(14) Fratev, F.; Miranda-Arango, M.; Padilla, E.; Sirimulla, S. *bioRxiv* **2019**,

(15) Small-Molecule Drug Discovery Suite 2017-4, Schrödinger, LLC, New York, NY, 2018. `https://www.schrodinger.com/`.

(16) Lema, C.; Varela-Ramirez, A.; Aguilera, R. J. *Current cellular biochemistry* **2011**, *1*, 1–14.

(17) Robles-Escajeda, E.; Das, U.; Ortega, N. M.; Parra, K.; Francia, G.; Dimmock, J. R.; Varela-Ramirez, A.; Aguilera, R. J. *Cellular Oncology* **2016**, *39*, 265–277.

(18) Sterling, T.; Irwin, J. J. *Journal of Chemical Information and Modeling* **2015**, *55*, 2324–2337.

(19) Merchant, A. A.; Jorapur, A.; McManus, A.; Liu, R.; Krasnoperov, V.; Chaudhry, P.; Singh, M.; Harton, L.; Agajanian, M.; Kim, M.; Triche, T. J.; Druker, B. J.; Tyner, J. W.; Gill, P. S.; Gill, P. S. *Blood advances* **2017**, *1*, 1635–1644.

(20) Lopes-Coelho, F. et al. *Oncotarget* **2017**, *8*, 82803–82823.

(21) Mu, X. et al. *Oncotarget* **2017**, *8*, 13174–13185.

(22) Wang, L. et al. *Journal of the American Chemical Society* **2015**, *137*, 2695–2703, PMID: 25625324.

(23) Fratev, F.; Sirimulla, S. *ChemRxiv* **2018**,

(24) Severson, A. F.; Meyer, B. J. *eLife* **2014**, *3*.

(25) Kallan, N. C. et al. *Bioorganic & Medicinal Chemistry Letters* **2011**, *21*, 2410–2414.

Figures

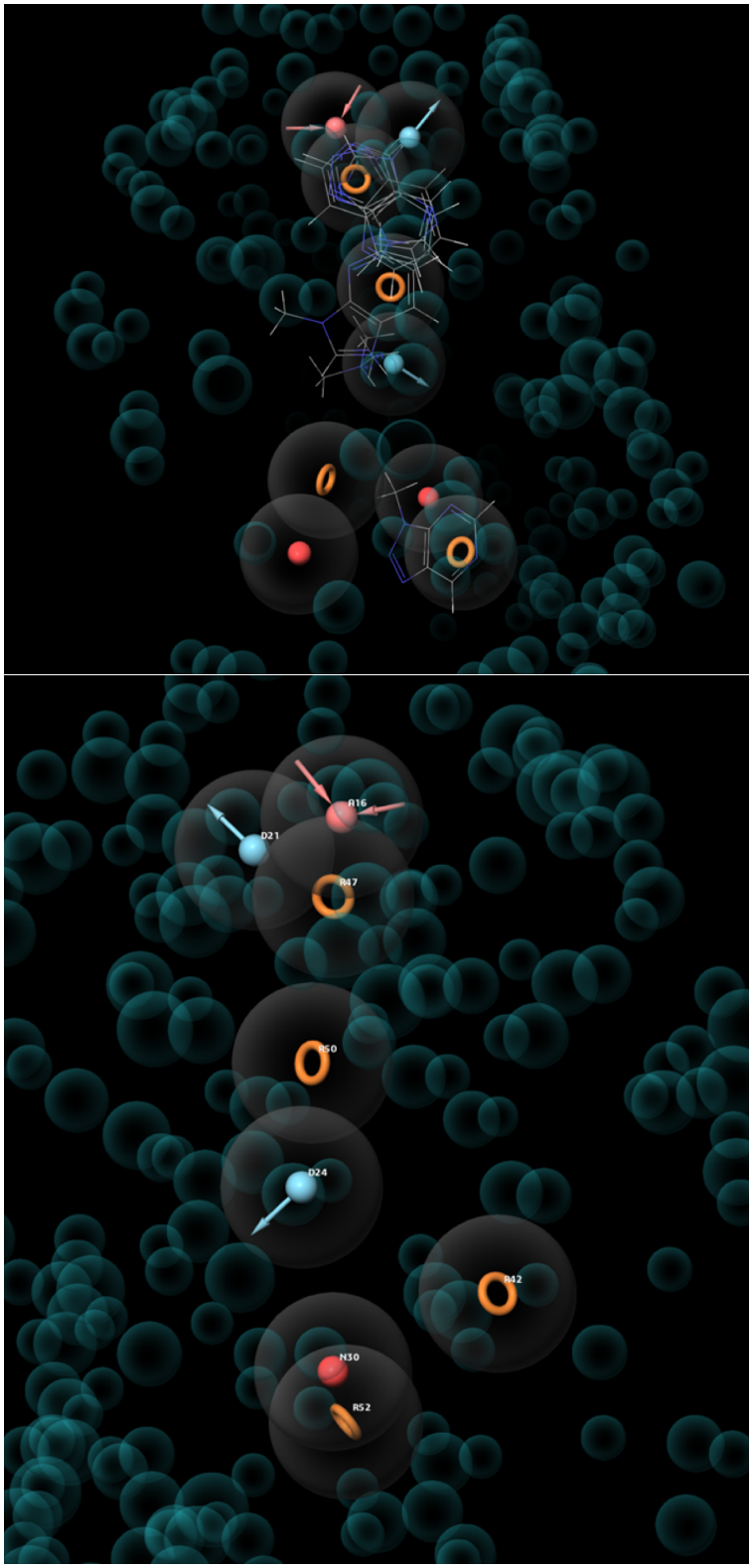

Figure 1: Pharmacophores [acceptor (pink), negative charge (red), aromatic ring (orange), and donor (blue)] are represented as solid spheres and donouts, excluded volumes are represented by spheres and some of the fragments that generated these points are also shown.(Top) Structure-based pharmacophore model of AKT with 9 pharmacophore points based on MD generated AKT structure. (Bottom) Structure-based pharmacophore model employed in the study that contains with eight pharmacophores and generated by PDB ID 3QKK.

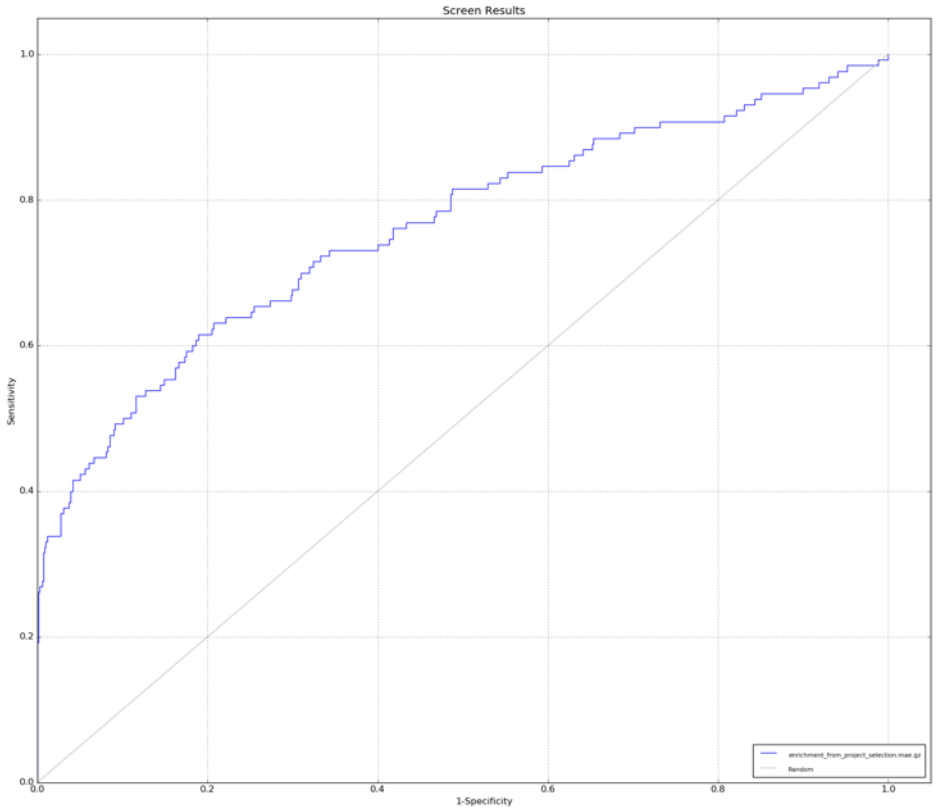

Figure 2: Recovery rate of the active ligands vs decoys achieved on the AKT1 subset, from the DUD-E set by a combination of Phase structure-based pharmacophore screen and Glide SP docking software, in the framework of Schrodinger 2017-4. X-axis represents 1-Specificity and Y-axis represents Sensitivity.

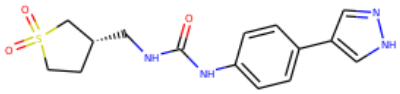

Compound 1: ZINC000095500624
Score = −9.1kcal/mol

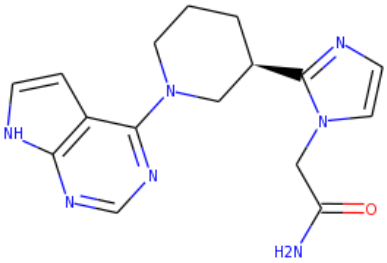

Compound 2: ZINC000095530701
Score = −9.0 kcal/mol

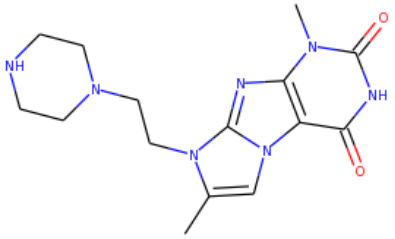

Compound 3: ZINC20706668
Score = −8.8 kcal/mol

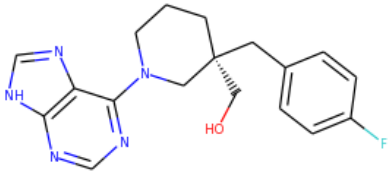

Compound 4: ZINC000067756373
Score = −8.7 kcal/mol

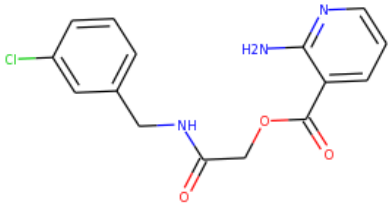

Compound 5 / Z18:
ZINC000024601677
Score = −9.0 kcal/mol

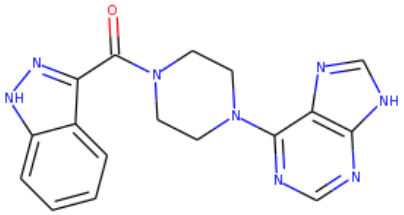

Compound 6: ZINC000071894354
Score = −9.2kcal/mol

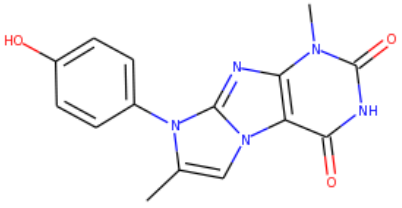

Compound 7: ZINC12549620
Score = −8.8kcal/mol

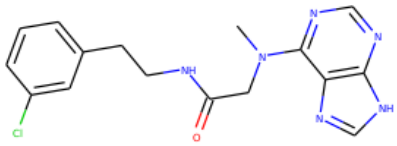

Z22: ZINC45978848
Score = −9.0 kcal/mol

Figure 3: VS-identified hits, confirmed by in vitro studies. Compound name, ZINC number, and docking score are also shown.

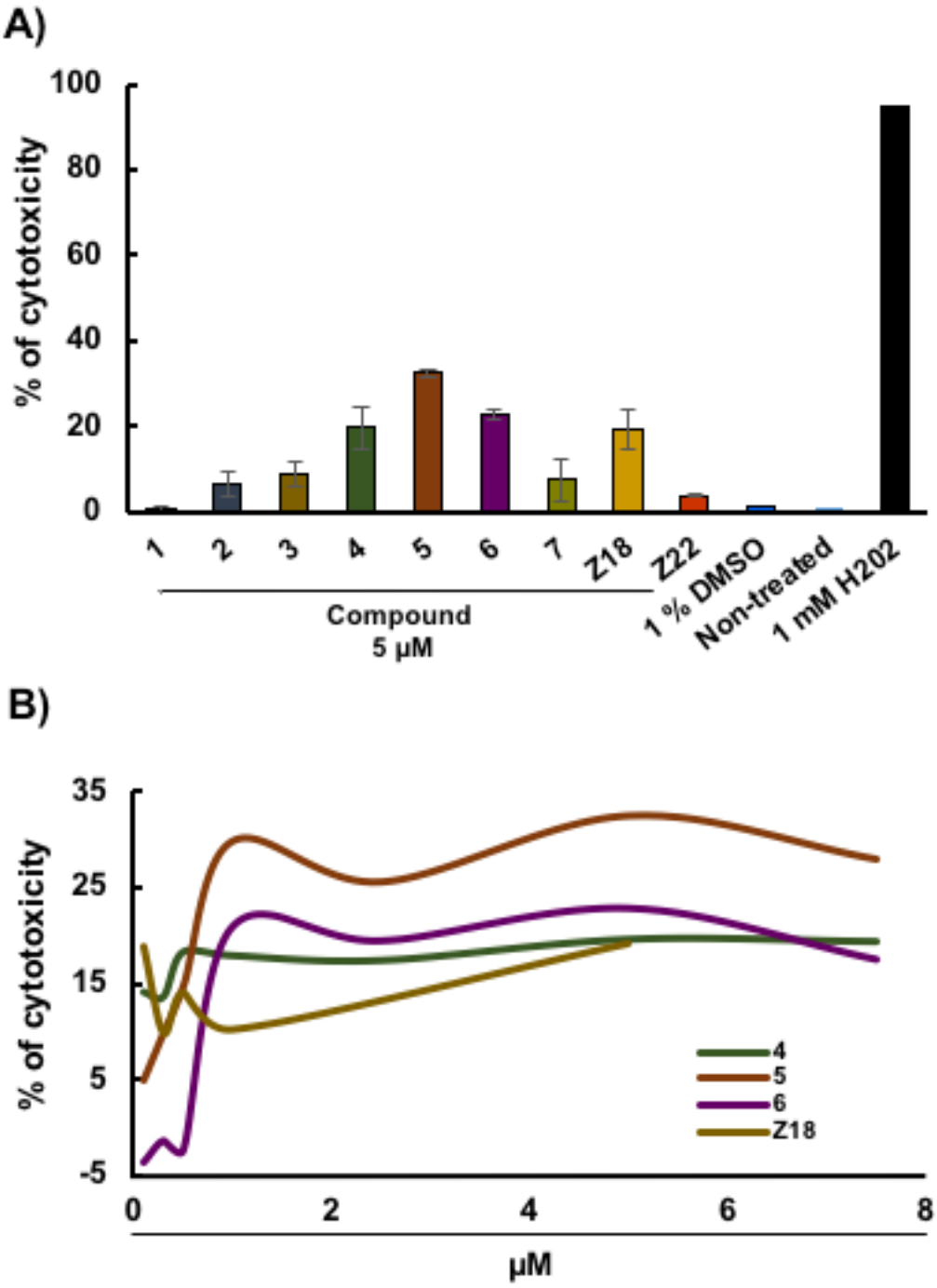

Figure 4: Analysis of the cytotoxic properties of compounds 5 and 6 against the acute lymphoblastic leukemia CEM cells. A differential nuclear staining assay (DNS) was employed to evaluate the cytotoxic activity of these compounds. Cells were exposed for 48 h at different concentrations of compounds 5 and 6, from 0.1 to 7.5 μM. A) Cytotoxicity values of CEM cells exposed to 5 μM of each compound. Compounds 4, 5, 6 and Z18 displayed the highest toxicity. B) Cytotoxicity dose-response curves of increasing concentrations of the experimental compounds 4, 5, 6 and Z18. Each plot represents an average of three experiments.

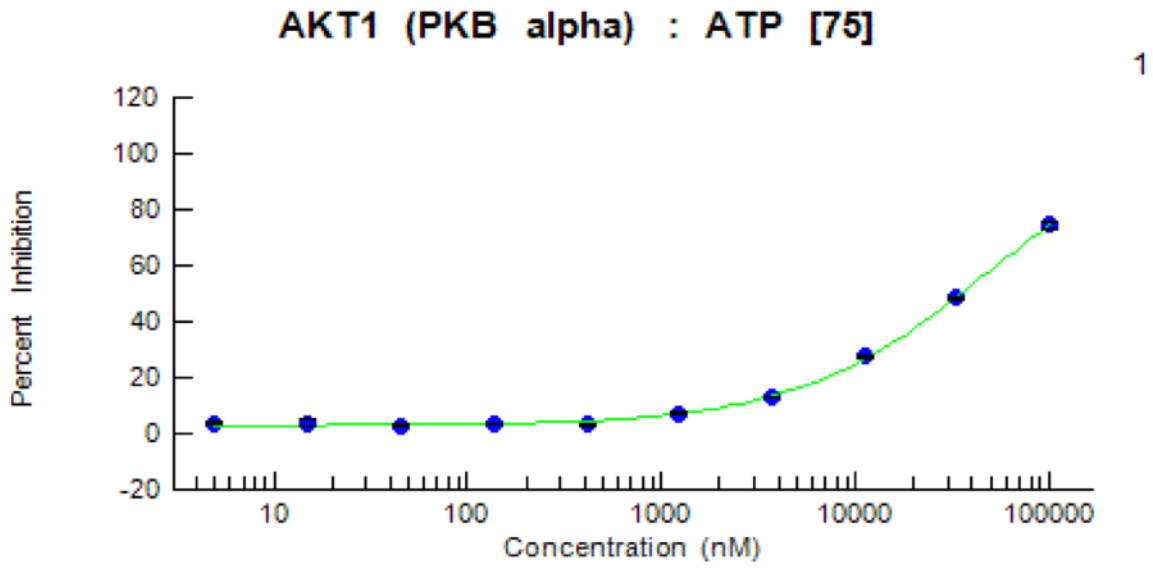

Figure 5: Ten-point AKT1 inhibition measurements for ligand 1. All values are based on experiments conducted twice.

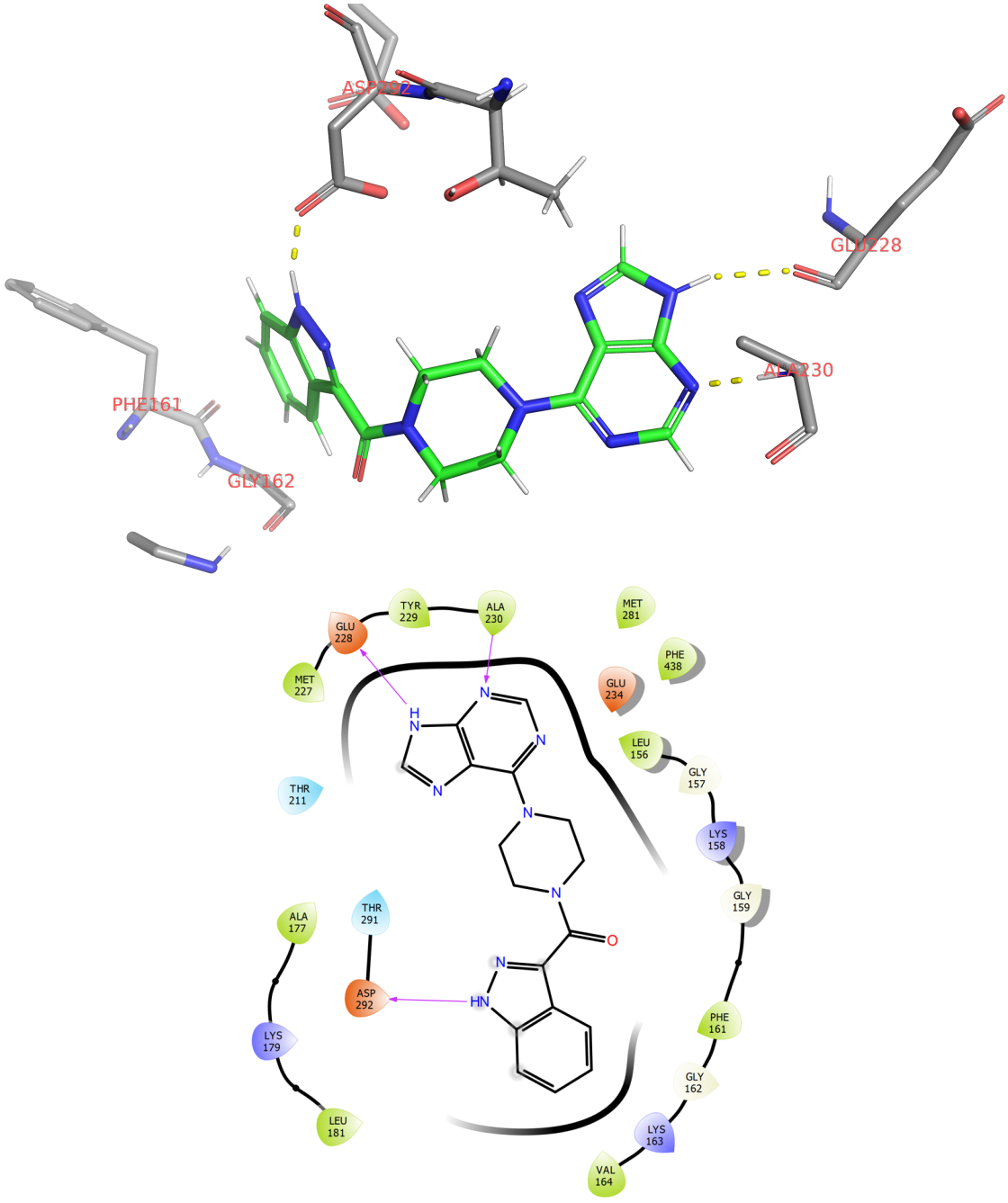

Figure 6: (A) 3D representation of compound 6-AKT1 interactions. Ligands are rendered in green stick models, interacting amino acids are rendered as grey stick models and Hydrogen bonds indicated in yellow dotted lines. (B) 2D representation of compound 6-AKT1 interactions, as identified by our docking studies.

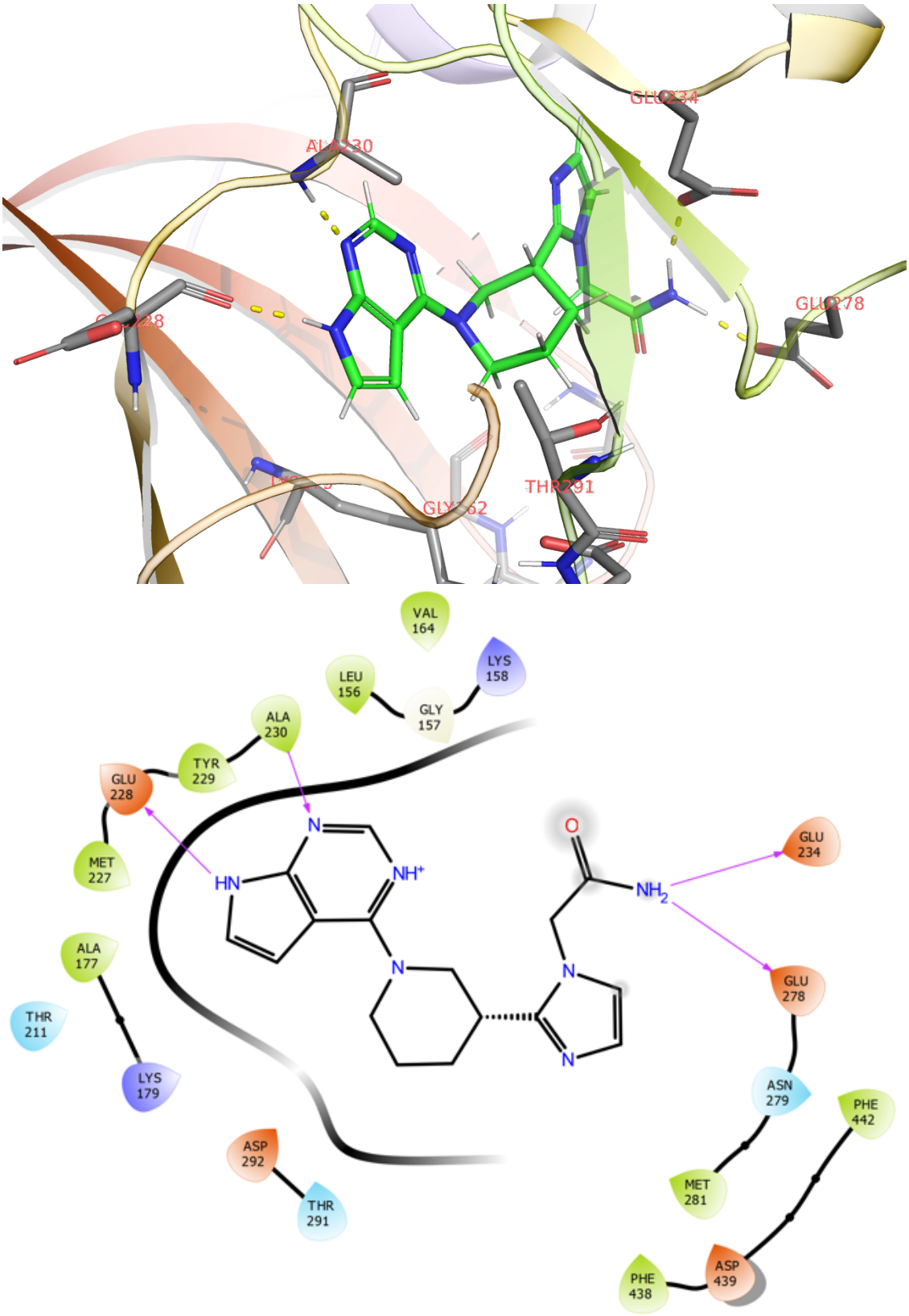

Figure 7: (A) 3D representation of compound 2-AKT1 interactions. Ligands are rendered in green stick models, interacting amino acids are rendered as grey stick models and Hydrogen bonds indicated in yellow dotted lines. (B) 2D representation of compound 2-AKT1 interactions, as identified by our docking studies.

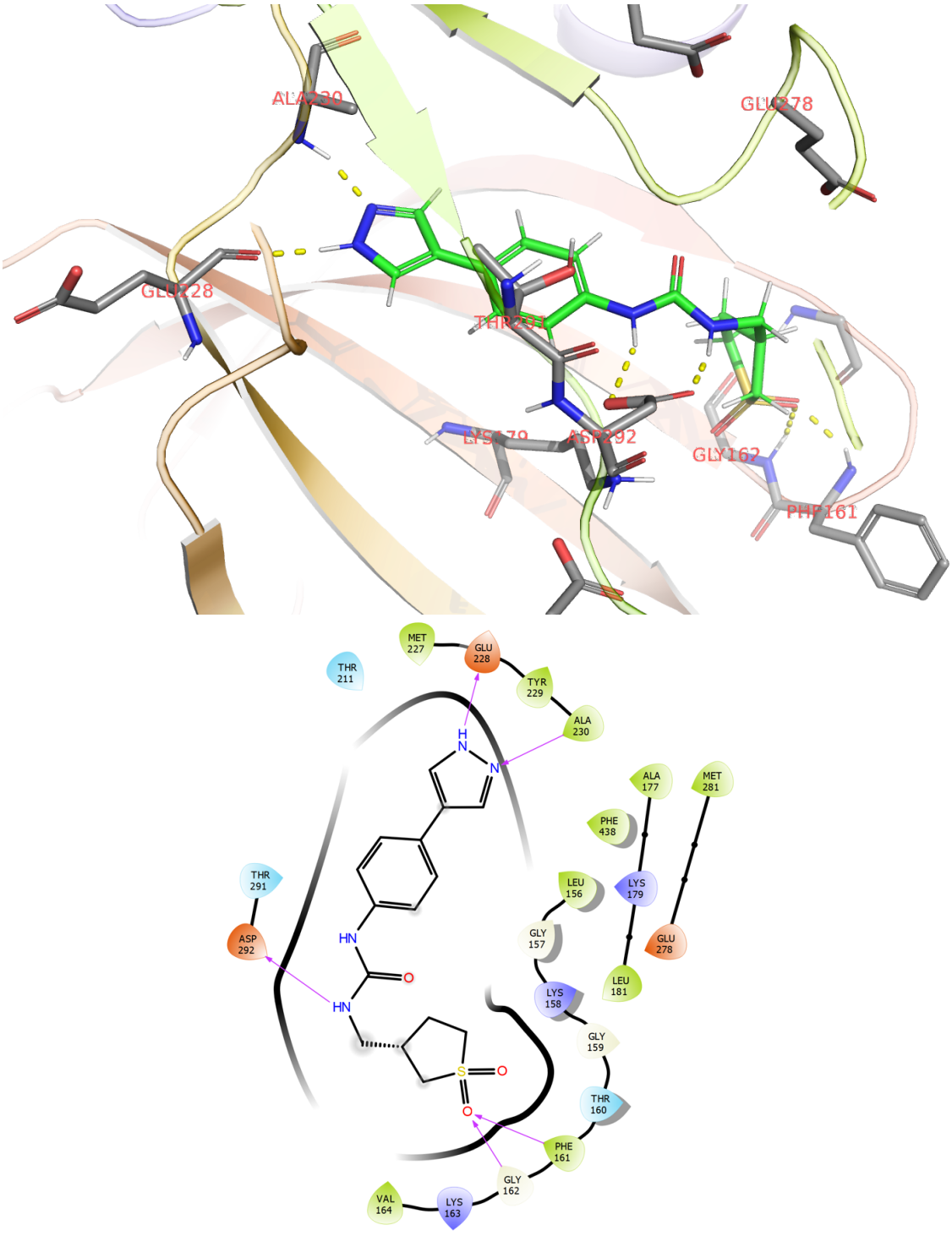

Figure 8: (A) 3D representation of compound 1-AKT1 interactions. Ligands are rendered in green stick models, interacting amino acids are rendered as grey stick models and Hydrogen bonds indicated in yellow dotted lines. (B) 2D representation of compound 1-AKT1 interactions, as identified by our docking studies.